aerospace

MDPI

Article

The Effect of 0–8 MPa Environmental Pressure on the Ignition and Combustion Process of CL20/NEPE Solid Propellant

Wenxiang Cai *, Wei Li and Zhixiang Wang

Key Laboratory of Special Engine Technology, School of Mechanical Engineering, Nanjing University of Science and Technology, Nanjing 210094, China; lw_9807@njust.edu.cn (W.L.); wzx_0205@njust.edu.cn (Z.W.)
* Correspondence: caiwx_2005@njust.edu.cn

Abstract: In order to study the effect of pressure on the ignition and combustion process of CL-20/NEPE solid propellant, the ignition delay, burning rate, and maximum combustion temperature of different solid propellant formulations with an ambient pressure of 0.1~8.0 MPa were measured experimentally by a solid propellant laser ignition experiment system, and the agglomeration process and the characteristics of condensed phase combustion products were analyzed. The experimental results show that, with the increase of pressure, the ignition-delay time decreases, and the burning rate and the maximum combustion temperature increase. With the increase of pressure, the influence on propellant ignition and combustion characteristics becomes smaller. In the experiment, the dynamic agglomeration phenomenon of aluminum particles in the propellant was recorded by a high-speed camera combined with a microscopic camera lens, and the dynamic agglomeration phenomenon of the combustion surface of the propellant and the dynamic agglomeration phenomenon, after the initial agglomeration was separated from the surface, were analyzed and expounded. Based on the experiment and combined with the agglomeration phenomenon, a mathematical model capable of predicting the particle size of aluminum aggregates was proposed.

Keywords: solid propellant; ambient pressure; ignition; agglomeration; mathematical model

Citation: Cai, W.; Li, W.; Wang, Z. The Effect of 0–8 MPa Environmental Pressure on the Ignition and Combustion Process of CL20/NEPE Solid Propellant. *Aerospace* **2024**, *11*, 672. https://doi.org/10.3390/aerospace11080672

Academic Editor: Jae Hyun Park

Received: 13 June 2024
Revised: 31 July 2024
Accepted: 14 August 2024
Published: 15 August 2024

1. Introduction

NEPE propellant, which stands for nitrate ester plasticized polyether propellant, was successfully developed in the United States at the end of the 1970s and began being used in the early 1980s. NEPE propellant combines the advantages of traditional composite solid propellants and double-base propellants, such as good low-temperature mechanical properties, high energy, and long service life. It also contains high amounts of high-energy explosives, such as Octogen (HMX) and Cyclotrimethylenetrinitramine (RDX), to meet the high-energy and high-performance requirements of modern solid rocket engines. Adding metal and aluminum particles to NEPE propellant can increase the specific impulse and strengthen combustion stability, but the accumulation, aggregation, and agglomeration of aluminum particles affect the further improvement of combustion efficiency. The condensed phase combustion products will lead to strong erosion and ablation, affecting the safety of engine operation [1]. Therefore, analyzing the ignition and combustion characteristics of NEPE propellants under various conditions, both inherent and external, and studying their energy-conversion process and efficiency are of great significance.

The ignition and combustion process of the propellant has a significant impact on the internal ballistics of solid rocket engines. Many scholars have conducted research on the ignition and combustion process of solid propellants and their performance in the early stages. This research provides valuable insights into the ignition and combustion mechanisms of solid propellants and serves as a reference for establishing or validating models of solid propellant ignition and combustion. The experimental results of Gnanaprakash et al. [2] show that the burning rate of 5 μm ammonium perchlorate (AP) particles is higher than that of 45 μm, and the effect of nano-Al on the burning rate is small. Li et al. [3] showed that

the ignition delay of aluminum–magnesium oxygen-poor propellants decreased with the increase in pressure and oxygen concentration, and the effect of oxygen content was significantly stronger than that of pressure. Guo et al. [4] found that the addition of fluorinated compounds to Butadiene propellants can effectively inhibit the agglomeration of aluminum particles, and the addition of low aluminum content and fluorinated organic matter is conducive to the improvement of the burning rate of hydroxyl-terminated polybutadiene (HTPB) propellants.

The agglomeration of aluminum particles in propellants has a significant impact on engine safety, leading many scholars to focus on studying the agglomeration dynamics of aluminum particles during the combustion process of propellants. Takahashi et al. [5] found that the decrease in the burning rate and the increase in aluminum particle brightness would lead to an increase in the agglomeration diameter. Liu et al. [6–8] used optical photography methods to measure the diameter of aluminum droplets in the flame front and in the flow motion and calculated their flow velocity. Ao et al. [9] used high-speed optical photography to study the agglomeration behavior of aluminum particles and the flame asymmetry of burning aggregates at 5 MPa. Li et al. [10] photographed the secondary agglomeration process of aluminum agglomeration products after they were removed from the combustion surface by an optical photographing method. Yuan et al. [11] captured the breakup of agglomerated droplets and the ejection of liquid aluminum oxide through photography. Tu et al. [12–14] used high-speed optical photography to capture the secondary agglomeration process of aluminum particles on and near the propellant-burning surface and analyzed the size changes of the agglomerates. The research results of Liu et al. [15] show that adding organic fluorine compounds to solid propellants will reduce the particle size of condensed products. Zhou et al. [16] added different amounts of organic fluorine to HTPB propellants, and the experiment showed that the addition of organic fluorine as an additive was helpful in reducing agglomeration in the combustion products of aluminized HTPB propellants. Gallier [17] proposed a random pocket model to predict the agglomeration size and agglomeration fraction of aluminum on the propellant-burning surface.

Due to the need for solid rocket engines to operate in environments with low air pressure and low oxygen content, these environmental factors have a certain impact on the ignition and combustion characteristics of the propellants. Currently, there is limited research on the ignition and combustion characteristics of solid propellants under different environmental conditions, and the underlying mechanisms are not sufficiently explored. Furthermore, during the combustion process of the propellant, due to the complexity of the agglomeration phenomenon, the aggregation mechanism remains unclear, and the models still have deficiencies. The agglomeration mechanism of aluminum particles needs further investigation to become clearer.

Therefore, this study uses a CO_2 laser ignition device to experimentally investigate the effects of environmental pressure ranging from 0 to 8 MPa and the size distribution of CL20-NEPE propellant particles on the ignition and combustion characteristics and the agglomeration behavior. The study aims to establish an agglomeration physical model by combining experimental results with theoretical analysis, with the goal of providing practical support for improving the operational performance of solid rocket engines and optimizing propellant formulations.

2. Experimental Research Methods and Objects

The solid propellant laser ignition experiment system is mainly composed of a laser control system, CO_2 laser, optical path system, combustion chamber, data-acquisition system, etc. The schematic diagram is shown in Figure 1. On the basis of that, an infrared thermal imager (FLIR A615, FLIR Systems, located in Wilsonville, OR, USA), fiber spectrometer (AvaSpec-ULS4096CL-EVO, Avantes, located in Eerbeek, The Netherlands), high-speed camera (Chronos 1.4, Krontech Canada Inc., located in Oakville, ON, Canada), micro-high-speed camera (OKA, located in Wuzhou, China), scanning electron microscope,

X-ray spectrometer (Hitachi HITACHI SU3500, Hitachi, located in Tokyo, Japan), X-ray diffractometer (D8 Advance, Bruker, located in Karlsruhe, Germany), laser particle size analyzer (Mastersize 3000, Malvern Panalytical, located in Malvern, Worcestershire, UK), and other measuring and analysis equipment to analyze the ignition combustion process, combustion products, and agglomeration process parameters were used.

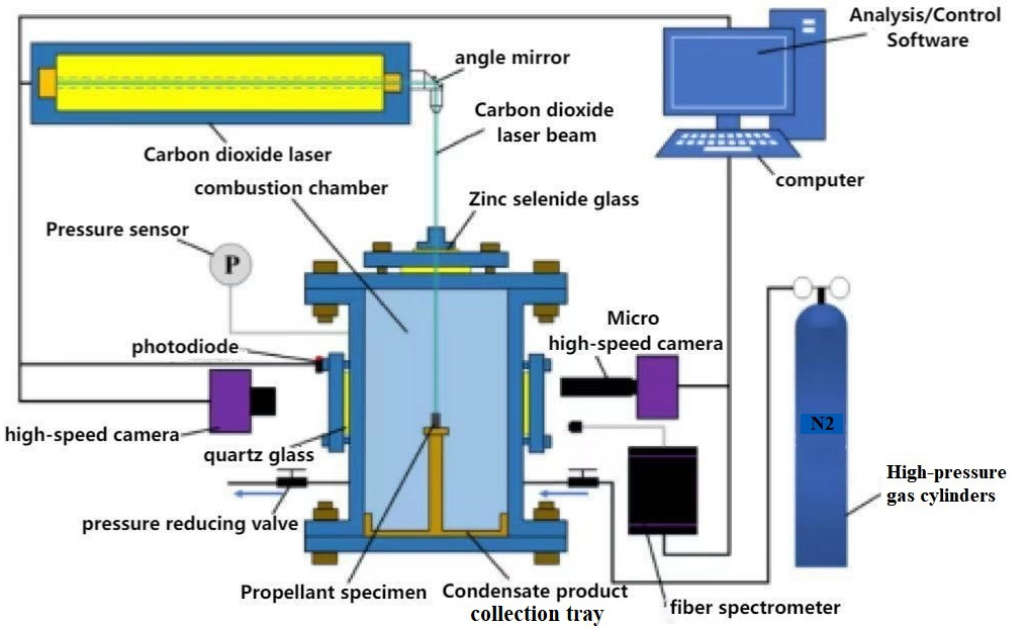

Figure 1. Schematic diagram of the experimental system.

2.1. Measuring Device and Testing Methods

The parameters of the data-measurement equipment (high-speed camera, microscopic high-speed camera, infrared thermal imager, and optical fiber spectrometer) are listed in Table 1.

Table 1. Parameters of data acquisition equipment for laser ignition and combustion experiments.

Instrument	Model	Parameter
High-speed camera	Chronos 1.4	resolving power 1280 × 1024@1000 FPS
Telephoto microscope lens	XDC-10A	Working distance 95 mm
Fiber spectrometer	AvaSpec-ULS4096CL-EVO	Wavelength range 200–1100 nm; Resolution 0.05–20 nm
Infrared thermal imager	FLIR A615	Temperature range +300 to +2000 °C; 200 FPS frame rate, transmitting 16-sbit images

In addition, the characteristics of the combustion products collected after the experiment were analyzed by a variety of measuring instruments, such as scanning electron microscopy, X-ray energy spectrometer, laser particle size analyzer, thermogravimetric analyzer (TGA/SDTA851E, Mettler Toledo, located in Zurich, Switzerland), X-ray diffractometer, etc. The models of test and measurement equipment used in this paper are shown in Table 2.

Table 2. Test equipment parameters.

Measuring Equipment	Model	Parameter
Scanning electron microscope and X-ray spectroscopy combined equipment	Hitachi HITACHI SU3500	SEM magnification 5–300 k
laser particle size analyzer	Mastersize 3000	Particle size range: 0.01–3500 μm
TGA	TGA/SDTA851E	Heating at a rate of 10 °C/min
X-ray diffractometer	D8 Advance	Angle reproducibility ± 0.0001°

2.2. Research Objects and Their Physical Properties

The NEPE propellants studied in this paper are mainly composed of glycidyl azide polymer (GAP), AP, hexanitrohexaazaisowurtzitane (CL-20), HMX, aluminum particle (Al), etc. The differences in the different formulations are shown in Table 3. The experimental samples are 5 mm × 5 mm × 10 mm cuboid, except the upper-end surface of 5 mm × 5 mm, which is coated with a flame retardant layer.

Table 3. Types of solid propellant specimens.

Sample Code	Illustrate
A-1	Basic formula (Al particle size 3 μm. AP particle size 250 μm. CL-20 & HMX particle size 250 μm)
A-2	Al particle size 30 μm
A-3	CL-20 & HMX particle size 100 μm
A-4	AP particle size 350 μm
A-5	AP particle size 450 μm
A-8	Plasticization ratio 2.1
A-9	Plasticization ratio 2.9

The ignition and combustion process of solid propellant is represented by five regional combustion wave profiles, as shown in Figure 2. Based on the steady-state combustion model of solid propellant, the flame-propagation process is analyzed. Figure 2 shows the flame-evolution process of different ignition and combustion stages of the base formula under an N2 atmosphere pressure of 8.0 MPa, which is mainly divided into five stages: initial ignition, combustion development, stable combustion, combustion decay, and flame quenching.

During the initial ignition stage (Figure 2a), the surface of the propellant is heated by laser irradiation, the temperature of the condensate phase continues to rise, the solid phase melts, and the condensate phase is decomposed, evaporates into the gas phase zone, and mixes with the ambient gas. When oxidants and adhesives continue to decompose, a large amount of active substances accumulate in the gas phase zone. When the time is long enough, the substances in the gas phase are ignited, and sporadic flames gradually appear. The decomposition of AP is further promoted, and upward jet gas products are formed [18]. The initial ignition stage transformed into a combustion-development stage 5 ms later (Figure 2b), after which the flame brightness became stronger, wider, and higher, and the combustion intensity and flame temperature gradually increased [19]. At the same time, the white smoke around the flame is also rising and increasing in concentration. More bright particles were observed to fly out of the high-temperature flame, mainly because, when the aluminum particles were released from the propellant surface, they were aggregated to form aluminum aggregates during combustion. And some aluminum particles that did not participate in the reaction were ejected with the airflow. As the mass to flux and thermal feedback gradually reach equilibrium, the combustion intensity reaches the maximum 51 ms after entering the combustion-development stage and enters the stable combustion stage (Figure 2c). This is where the flame shape remains basically unchanged, and a large amount of white smoke surrounds the flame. With the consumption of the oxidizer, the flame enters the combustion-decay stage (Figure 2d), and the flame height gradually decreases. The white smoke concentration decreases and slowly disperses until it enters the flame-quenching stage (Figure 2e), and the flame area gradually decreases until it is extinguished. On the whole, the propellant flame develops quickly, and the rate of extinction is relatively slow.

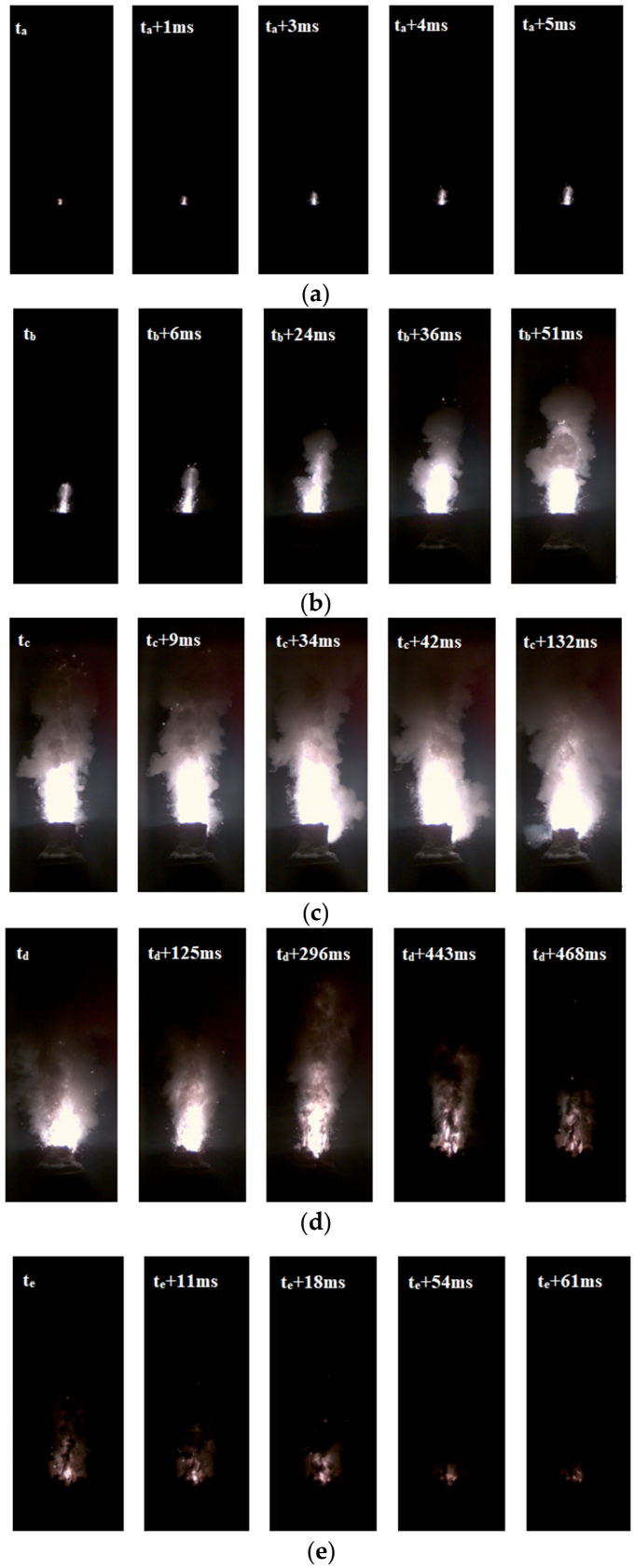

Figure 2. Flame-evolution process of ignition combustion. (**a**) Initial ignition stage. (**b**) Combustion-development stage. (**c**) Stable combustion stage. (**d**) Combustion-decay stage. (**e**) Flame-quenching stage.

3. Influence of Environmental Pressure on Ignition and Combustion Characteristics

The ignition delay, burning rate, maximum combustion temperature, and spectral characteristics of different solid propellant formulations with ambient pressures of 0.1~8.0 MPa were measured experimentally.

The flame temperature distribution in the combustion field is one of the important parameters to measure the energy of solid propellants. Figure 3 presents the temperature distribution of the combustion wave obtained using an infrared thermal imager during stable combustion of the propellant. The maximum temperature in this temperature field represents the highest temperature throughout the entire combustion process. Figure 3a,b depicts the conditions under 1.0 MPa pressure in air and nitrogen atmospheres, respectively. The flame structure and temperature distribution remain largely unchanged between the two environments. However, as the oxygen concentration in the environment increases, the combustion reaction becomes more intense, leading to an increase in the peak temperature of the combustion wave. Figure 4 shows the change in the maximum temperature of the flame combustion wave with pressure. It can be seen from the figure that, with the increase in pressure, the increase of the solid propellant burning rate is smaller than the change in the oxygen concentration per unit volume in the environment. So, as the relative oxygen-fuel ratio in unit volume increases, the time to reach the burning surface temperature and adiabatic flame temperature becomes shorter. And the combustion reaction is more intense, and the reaction rate is faster. At this time, the variation law of the maximum temperature obtained by fitting the quadratic function with the environmental pressure is shown in Equation (1), and the variance is 0.99016.

$$y = 1506.6968 + 0.63743x + 7.96343x^2 \; R^2 = 0.99016 \tag{1}$$

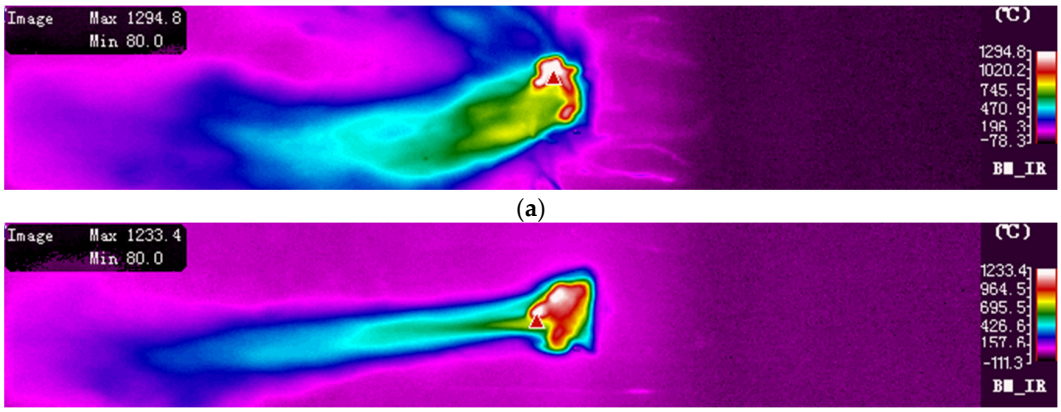

Figure 3. Maximum combustion temperature field under different ambient atmospheres of 1.0 MPa. (**a**) Air. (**b**) N_2.

The ignition-delay time t_{ig} is the time from the start of external excitation to the start of sustained propellant combustion. It is mainly composed of the pyrolysis time (t_{py}) from the beginning of the propellant combustion surface to the lowest value required for the pyrolysis to ignite, the diffusion mixing time (t_{mix}) required for the mixture of the vapor formed by pyrolysis and the ambient gas to achieve the ignition conditions, and the gas phase chemical reaction time (t_{chem}) required for the combustion of the pyrolyzed fuel gas at the ignition source [20].

$$t_{ig} = t_{py} + t_{mix} + t_{chem} = \frac{\pi \rho_t c k \left(T_{py} - T_0\right)^2}{4{q_0}^2} + \frac{k^2}{{h_c}^2 D} + \frac{CkT_\infty}{\alpha[E/(RT_\infty)]\Delta h_c A e^{-E/(RT_\infty)}} \tag{2}$$

where T_{py} is the pyrolysis temperature, C is the constant coefficient, E is the activation energy, R is the universal gas constant, Δh_c is the combustion heat, A is the prefactor,

α is the thermal diffusion coefficient of the mixed gas, D is the diffusion coefficient, h_c is the convective heat-transfer coefficient, and ρ_t is the solid phase density. T_0 is the initial temperature, c is the specific heat capacity, k is the thermal conductivity, and q_0 is the laser heat flux. For a given propellant, where the laser heat flux is known, t_{py} is constant.

The increase in pressure increases the collision between chemical molecules of the pyrolysis products and the reaction rate, intensifies the chemical reaction on the surface of the propellant, and increases the heat-transfer efficiency, which leads to the reduction of the ignition-delay time. It can be seen from the above data that there is a certain critical pressure of the aluminum-containing NEPE propellant. Outside this pressure range, the influence of pressure on the ignition-delay time will become smaller.

Based on the mathematical model of ignition-delay time established by Li [20], this paper obtains the estimation model of ignition delay of CL20/NEPE propellant:

$$t_{ig} = Ap^B + C = 560039.36p^{-0.000665} - 559198.95 \quad (3)$$

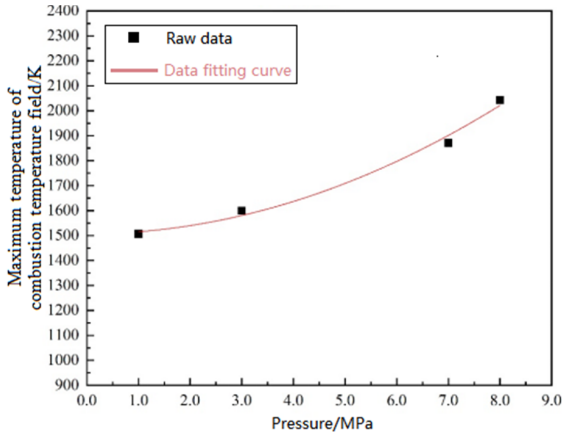

Figure 4. Curve of the highest temperature of combustion flame changing with pressure.

It can be seen from the Figure 5 that the pressure increases from 1.0 MPa to 7.0 MPa, and the ignition-delay time decreases from 780 ms to 111 ms. This is because the increase in pressure reduces the diffusion speed of the solution products to the periphery, increases the collision between chemical molecules and the reaction rate, and enhances the heat conduction efficiency, thus reducing the ignition-delay time.

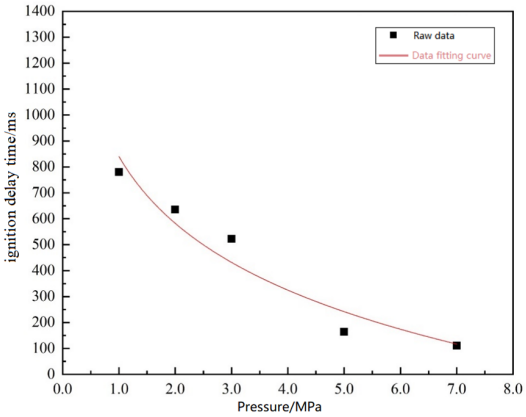

Figure 5. Fitting of ignition-delay time curves under different pressures of the basic formula.

4. Influence of Propellant Components on Ignition Combustion Process

In this chapter, we investigate the effects of different propellant compositions on ignition and combustion characteristics under environmental pressures ranging from

0.1 to 8.0 MPa at a constant temperature of 20 °C. This investigation involves altering the particle sizes of CL-20, Al, and AP. Through multiple experimental sets, we obtained error bar charts, which indicate that the experimental data have an error margin within 8%, are stable, exhibit low dispersion, and have a high degree of reliability.

4.1. Influence of CL-20 Particle Size

Figure 6 shows the burning rate of two propellants with different particle sizes of CL-20 as a function of pressure. As can be seen from the figure, A-3 propellant with coarse particle size CL-20 increases the combustion flame temperature of the propellant, resulting in the increase of gas–solid thermal feedback and the propellant burning rate. The range of burning rate increase is more obvious with the increase in pressure. In addition, the increase of CL-20 particle size causes the internal gap of the propellant to become larger, the degree of concaveness of the combustion surface to become larger, and the hot melt part of the adhesive can not easily cover the coarse-grained CL-20 completely. And the burning rate will increase.

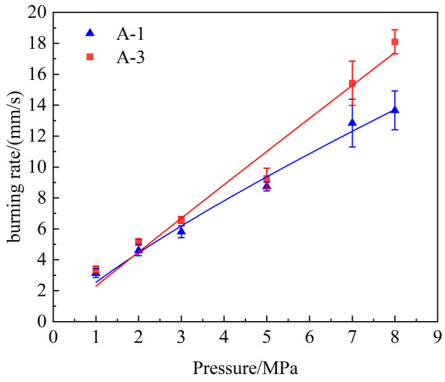

Figure 6. Effect of CL-20 particle size under different pressures on burning rate.

Figure 7 shows the change in the ignition-delay time of the two propellants when pressure changes. The ignition-delay time of A-3 propellants added with coarse-grained CL-20 is smaller than that of A-1 propellants. At low pressure and strong pressure, the ignition-delay time difference between the two is large, and with the increase in pressure, the ignition-delay time difference becomes smaller. This is because coarse-grained CL-20 produces more pyrolysis gas in the process of decomposition by heating, which shortens the inert heating time and leads to the reduction of ignition-delay time.

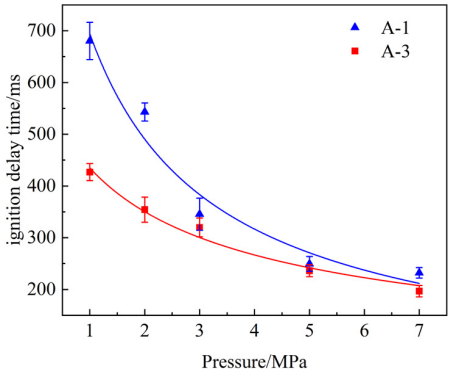

Figure 7. Effect of CL-20 particle size under different pressures on ignition-delay time.

Based on the exponential burning rate law, the burning rate of the two propellants was fitted according to Equation (3). It can be seen from Figure 6 that, to a certain extent, the burning rate and pressure index could be improved by appropriately increasing the CL-20 particle size when the principal component and content were unchanged.

It is obvious that the ignition-delay time of the two propellants is negatively correlated with the pressure. When the pressure increases from 1.0 MPa to 7.0 MPa, the ignition-delay time of the A-1 propellant decreases from 681 ms to 230.64 ms, while the ignition-delay time of the A-3 propellant decreases from 426.23 ms to 195.07 ms. To some extent, the sensitivity of the ignition-delay time of A-1 propellant containing medium-size CL-20 to pressure is greater than that of the A-3 propellant containing coarse-size CL-20.

4.2. Influence of Al Particle Size

Figure 8 shows the fitting curve of the burning rate of propellants with different particle sizes. With the increase in pressure, the burning rate difference between the two propellants becomes larger, which is due to the change in the combustion and thermochemical behavior of Al particles, which generally includes the pyrolysis of the CH_2O group when the thermal decomposition is greater than 5.0 MPa, resulting in the increased rate of the burning rate at high pressure being much greater than that at low pressure.

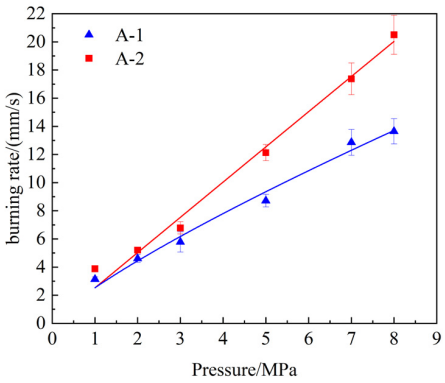

Figure 8. Effect of pressure on burning rate of Al propellants with different particle sizes.

Figure 9 shows the comparison of the ignition-delay time of propellants containing different particle sizes of Al particles. Similarly, with the increase in pressure, A-2 propellants containing coarse-grained Al particles speed up the pyrolysis of oxidants, and the concentration of thermal decomposition products reaches the ignition conditions faster. So, the ignition-delay time is smaller under different pressures.

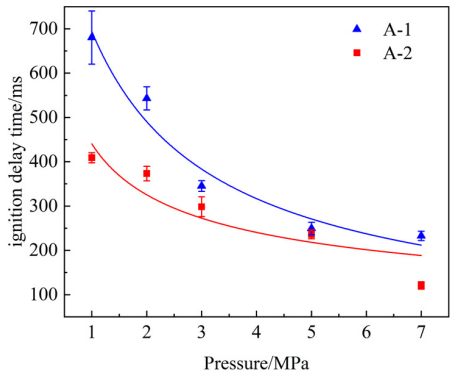

Figure 9. Fitting curves of ignition-delay time of A-1 and A-2 propellants with pressure variation.

4.3. Influence of AP Particle Size

Figure 10 shows the fitting curves of burning rates of A-1 and A-5 propellants with different particle sizes of AP under a nitrogen atmosphere. It is very obvious that the burning rate of propellants with different particle size APs is positively correlated with pressure. As the pressure increases from 1.0 MPa to 8.0 MPa, the burning rate of the A-1 propellant with an AP particle size of 250 μm increases from 3.11 mm/s to 13.58 mm/s,

while the burning rate of the A-5 propellant with an AP particle size of 450 μm increases from 3.10 mm/s to 12.77 mm/s. In comparison, the effect of AP particle size on the burning rate of the propellant is not obvious, and the burning rate of the A-5 propellant with a coarser AP particle size (450 μm) is slightly lower than that of the A-1 propellant with a medium AP particle size (250 μm) under each pressure condition.

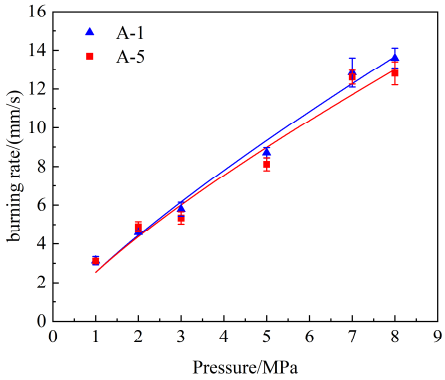

Figure 10. Fit curve of burning rate for two propellants with different particle sizes of AP.

5. Research on Combustion and Agglomeration Characteristics of Aluminum Particles

5.1. Analysis of Aluminum Particle Agglomeration Process

The agglomeration of aluminum particles on the propellant's combustion surface and the escape of aggregates under different pressure conditions are shown in Figure 11. Among them, the agglomeration morphology of aluminum particles at 0.1 MPa was coral-like. These coral-like materials are formed by melting and condensation of aluminum particles. With the increase in temperature, coral-like materials accumulate and aggregate upward on the burning surface, and small coral-like materials merge to form larger coral-like aggregates. The coral-like morphology is maintained for a long time.

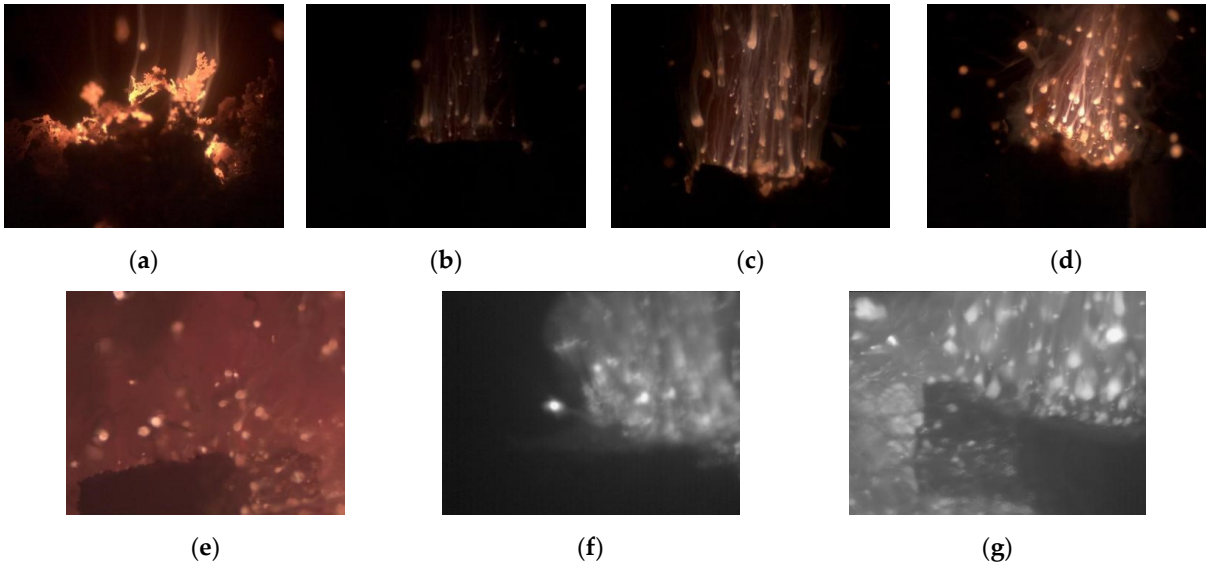

Figure 11. Agglomeration and escape of aluminum particles on the combustion surface under different pressures. (**a**) 0.1 MPa, (**b**) 1.0 MPa, (**c**) 2.0 MPa, (**d**) 3.0 MPa, (**e**) 5.0 MPa, (**f**) 7.0 MPa, and (**g**) 8.0 MPa.

With the increase in pressure, the existence time of the coral-like morphology decreases continuously, and the initial aggregates formed by accumulation, aggregation, and agglomeration on the burning surface "devour" the newly exposed aluminum particles or merge with other initial aggregates to form larger aggregates. During the whole process

of agglomeration formation, the initial agglomeration moves in various trajectories and directions and merges and fuses with aggregates of different sizes near or far from the combustion surface of the propellant. It is also found that, with the increase in environmental pressure, the time of initial agglomeration on the combustion surface becomes shorter, and the velocity of the initial agglomeration on the combustion surface becomes faster. It is also observed that the aggregate particles gradually become brighter, which is due to a certain increase in the surface temperature of the aggregate. From the images of 0.1~8.0 MPa, it is obvious that the propellant produces more smoke during combustion, and the aluminum particles or aluminum aggregates sputtering from the surface of the propellant increase at the same time.

5.2. Particle Size and Agglomeration Model of Condensate Products

The most common agglomeration models include the experience model, the packaging model, the pocket model, etc. Among them, the pocket model is the most reasonable one that can explain the formation process of agglomeration more simply and reasonably [21]. Based on the principle of the pocket model and the experimental data, a pocket model for an Al/CL-20/NEPE propellant is proposed in this paper to better predict aggregate size.

Figure 12 shows the SEM scanning of the propellant surface, with large AP particle sizes and micron aluminum powder and additives around it. In this figure, pits generated by AP particles falling off can be regarded as AP particles, which can improve the accuracy of the pocket model [20]. Accordingly, the spherical region of the AP particle envelope is regarded as a pocket, and the diameter of the pocket is approximately equal to the diameter of the spherical region. All aluminum particles in the pocket are aggregated into larger aluminum aggregates. The pocket model is established as shown in Figure 13 and can be calculated using Equation (4).

$$D_{\text{pocket}} = \gamma D \tag{4}$$

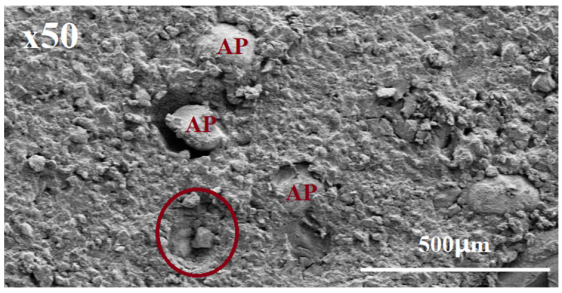

Figure 12. SEM image of AP distribution on propellant surface.

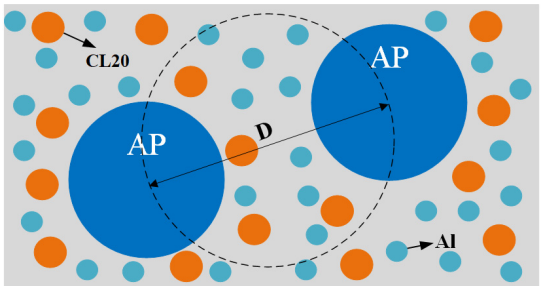

Figure 13. Schematic diagram of pocket model.

Among them, γ is the correction coefficient introduced to consider the influence of space occupied by AP particles within the diameter D_{pocket} range [22], which is related to the pocket diameter D_{pocket} and AP particle diameter D_{AP}, and can be calculated by Equation (5).

$$\gamma = (1 - Y_{\mathrm{AP}})^{1/3} \tag{5}$$

In the above formula, Y_{AP} is the AP particle volume fraction. Assuming that all the contained aluminum particles in the pocket form a large-sized aggregate, the volume fraction of the components in the propellant is calculated as follows:

$$Y_{\mathrm{AP}} = \frac{\varepsilon_{\mathrm{AP}} \times \rho_{\mathrm{P}}}{\rho_{\mathrm{AP}}} \tag{6}$$

$$Y_{\mathrm{Al}} = \frac{\varepsilon_{\mathrm{Al}} \times \rho_{\mathrm{P}}}{\rho_{\mathrm{Al}}} \tag{7}$$

$$Y_{\mathrm{CL20}} = \frac{\varepsilon_{\mathrm{CL20}} \times \rho_{\mathrm{P}}}{\rho_{\mathrm{CL20}}} \tag{8}$$

where ε_{AP}, ε_{Al}, and $\varepsilon_{\text{CL-20}}$ are the mass fraction of each component, and ρ_{AP}, ρ_{Al}, $\rho_{\text{CL-20}}$, and ρ_p represent the density of each component and propellant, respectively.

Assuming that aluminum and CL-20 particles are evenly distributed in the pocket, the volume fraction of the aluminum particles and the CL-20 particles can be expressed as Equations (9) and (10).

$$Y_{\mathrm{pocket,AP}} = \frac{Y_{\mathrm{Al}}}{1 - Y_{\mathrm{Al}}} \tag{9}$$

$$Y_{\mathrm{pocket,CL20}} = \frac{Y_{\mathrm{CL20}}}{1 - Y_{\mathrm{CL20}}} \tag{10}$$

According to this, the number of CL-20 particles $N_{\text{CL-20}}$ and the number of aluminum particles N_{A1} in the pocket can be calculated by the formula in Equations (11) and (12):

$$N_{\mathrm{CL20}} = \frac{D^3_{\mathrm{pocket}} \times Y_{\mathrm{pocket,CL20}}}{D^3_{\mathrm{CL20}}} \tag{11}$$

$$N_{\mathrm{Al}} = \frac{\left(D^3_{\mathrm{pocket}} - D^3_{\mathrm{CL20}} \times N_{\mathrm{CL20}}\right) Y_{\mathrm{pocket,Al}}}{D^3_{\mathrm{Al}}} \tag{12}$$

$D_{\text{CL-20}}$ and D_{Al} represent the original average particle size of the CL-20 and Al particles.

Sum the aluminum particles contained in the mouth bag and calculate the mass m_{Al} of aluminum particles contained in the outlet bag:

$$m_{\mathrm{Al}} = N_{\mathrm{Al}} \times \frac{\pi}{6} \times D^3_{\mathrm{Al}} \times \rho_{\mathrm{Al}} \tag{13}$$

Assuming that all the aluminum particles contained in the pocket only agglomerate to form a larger aggregate, the aggregated particle diameter is D_f:

$$D_f = \left(\frac{6 \times m_{\mathrm{Al}}}{\pi \times \rho_{\mathrm{Al,l}}}\right)^{1/3} \tag{14}$$

where $\rho_{Al,l}$ is the density of liquid aluminum.

In addition, this paper adopts the modified burning rate coefficient method proposed by Duterque [23] to consider the influence of the combustion process on the agglomeration process, and the modified aggregate diameter is expressed by the following formula.

$$D_{f-1} = (2.42/r) \times D_f \tag{15}$$

After the initial agglomeration is formed, several agglomerates will fuse with each other to form new agglomerates of a larger size before leaving the propellant's burning surface. After considering this factor, the model is introduced. In order to facilitate calculation, the coefficient a is introduced as the influence factor. In this model, a is 0.65. The size of the large-sized new aggregates formed by two initial aggregates of the same size that are most common is expressed as:

$$D_{f-2} = a^3 \sqrt{2\left(D_{f-1}\right)^3} \tag{16}$$

The prediction data of the model were compared with the experimental data to verify the rationality of the model. The propellant parameters used in the calculation are shown in Table 4.

Table 4. Relevant parameters of propellant.

Parameter	Numerical Value
ρ_{AP}	1.95×10^3 kg/m^3
ρ_{Al}	2.7×10^3 kg/m^3
ρ_{P}	1.64×10^3 kg/m^3
$\rho_{Al,l}$	2.35×10^3 kg/m^3
$\rho_{CL\text{-}20}$	2.04×10^3 kg/m^3
D	280 μm

Figure 14 shows the comparison between the results obtained from the Al/CL-20/NEPE propellant agglomeration model established in this paper and the experimental data. The prediction results of $D_{f\text{-}2}$ obtained by the prediction model are in good agreement with the experimental data. In the range of 3.0~8.0 MPa, with the increase in pressure, the prediction results of the prediction model tend to be consistent with the experimental results, and the error decreases continuously, which is only 1.37% at 8.0 MPa.

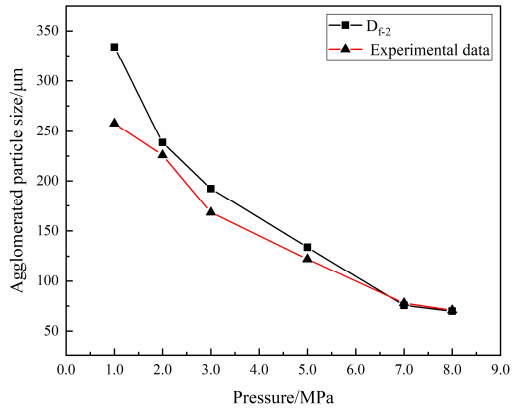

Figure 14. Comparison between experimental results and agglomeration model.

6. Conclusions

Due to the production of flammable gases and particle agglomerates during the ignition and combustion process of aluminum-containing NEPE propellants used in solid rocket engines, a complex two-phase flow combustion is formed, which has an impact on engine performance. Therefore, this study utilizes a solid propellant laser ignition system to investigate the ignition and combustion process and agglomeration characteristics of aluminum-containing NEPE propellants under various external and internal factors (different environmental and formulation conditions). The main research work and conclusions are as follows.

(1) The research results indicate that the evolution of the ignition and combustion flame process primarily consists of five stages, namely the initial ignition, combustion devel-

opment, stable combustion, combustion decay, and flame quenching. Additionally, the ignition-delay times at different pressures were fitted to a function, and the results show that, as the pressure increases, the ignition-delay time decreases. Furthermore, as the pressure increases, both the burning rate and the maximum combustion temperature increase. And the effect of pressure on the ignition and combustion characteristics of the propellant diminishes. The identified patterns provide a reference for future applications of propellants;

(2) The research results indicate that, as the particle size of the CL-20 in the propellant increases, it becomes more difficult for the CL-20 to be covered by the molten binder system. This results in a greater amount of pyrolysis gas being produced during the heating and decomposition process, leading to a decrease in the ignition-delay time and an increase in the burning rate. It was also found that the ignition-delay time of propellants containing coarse-grained CL-20 is less sensitive to changes in pressure. When the particle size of Al in the propellant is reduced, the interaction between Al particles and the oxidizer increases, leading to a higher heat release during the thermal decomposition reaction, stronger flame intensity, faster burning rate, and shorter ignition-delay time. When the particle size of AP in the propellant is decreased, the surface area of AP increases, promoting thermal decomposition, increasing heat feedback, and accelerating the burning rate. The study's findings have an error margin of no more than 8%, providing significant reference points for the design of propellant formulations;

(3) Using optical photography techniques and a combustion-product collection system, the agglomeration phenomena and the mechanisms of the propellant were analyzed. The study shows that, as the pressure increases, the duration of the coral-like morphology in the aluminum particle agglomeration process significantly decreases. And the number of aluminum particles escaping from the propellant combustion surface increases. By combining the various agglomeration behaviors of aluminum particles observed in the experiments, a physical model was established to comprehensively understand the formation process and principles of aluminum agglomerates. Based on the principles of the classical pocket model, a mathematical model was proposed to predict the size of agglomerates, and when comparing the experimental results with the predicted results, it was found that the predictive model had a high degree of agreement with the experimental data.

Author Contributions: Conceptualization, W.L. and Z.W.; methodology, W.C.; software, W.L.; validation, W.C., W.L. and Z.W.; formal analysis, Z.W.; investigation, Z.W.; resources, W.C.; data curation, W.L.; writing—original draft preparation, W.C.; writing—review and editing, W.L.; visualization, Z.W.; supervision, W.C.; project administration, W.C.; funding acquisition, W.C. All authors have read and agreed to the published version of the manuscript.

Funding: This research was funded by the National Natural Science Foundation of China grant number 51306092. And The APC was funded by the National Natural Science Foundation of China grant number 51306092.

Data Availability Statement: The data presented in this study are available upon request from the corresponding author due to the privacy concerns associated with textual research data.

Conflicts of Interest: The authors declare no conflict of interest.

References

1. Wu, X.; Chen, J.; Wang, D. *Principles of Solid Rocket Motor*; Arms Industry Press: Beijing, China, 2011.
2. Gnanaprakash, K.; Chakravarthy, S.R.; Sarathi, R. Combustion mechanism of composite solid propellant sandwiches containing nano-aluminium. *Combust. Flame* **2017**, *182*, 64–75. [CrossRef]
3. Li, L.B.; Chen, X.; Musa, O.; Zhou, C.S.; Zhu, M. The effect of pressure and oxygen concentration on the ignition and combustion of aluminum-magnesium fuel-rich propellant. *Aerosp. Sci. Technol.* **2018**, *76*, 394–401. [CrossRef]
4. Guo, Y.; Li, J.; Gong, L.; Xiao, F.; Yang, R.; Meng, L. Effect of Aluminum and Organic Fluoride on the Combustion Properties of Hydroxyl Terminated Polybutadiene Propellant. *Chin. J. Explos. Propellants* **2020**, *43*, 74–80.

5. Takahashi, K.; Oide, S.; Kuwahara, T. Agglomeration characteristics of aluminum particles in AP/AN composite propellants. *Propellants Explos. Pyrotech.* **2013**, *38*, 555–562. [CrossRef]
6. Liu, X.; Liu, P.J.; Jin, B. Experimental Study Methods for Combustion of Aluminum in Composite Propellants. *Solid Rocket Technol.* **2015**, *38*, 833–836.
7. Liu, X.; Liu, P.J.; Jin, B. Experimental Study on Aluminum Combustion in Composite Propellants. *J. Propuls. Technol.* **2016**, *37*, 1579–1585.
8. Liu, X.; Ao, W.; Liu, H.; Liu, P. Aluminum agglomeration on burning surface of NEPE propellants at 3–5 MPa. *Propellants Explos. Pyrotech.* **2016**, *42*, 260–268. [CrossRef]
9. Ao, W.; Liu, X.; Rezaiguia, H.; Liu, H.; Wang, Z.; Liu, P. Aluminum agglomeration involving the second mergence of agglomerates on the solid propellants burning surface: Experiments and modeling. *Acta Astronaut.* **2017**, *136*, 219–229. [CrossRef]
10. Li, L.; Chen, X.; Zhou, C.; Zhu, M.; Lai, J. Characteristics of Aluminium Particle Agglomeration in Aluminum-magnesium Oxygen-depleted Propellants. *Chin. J. Energetic Mater.* **2019**, *27*, 759–765.
11. Yuan, J.; Liu, J.; Zhou, Y.; Wang, J.; Xv, T. Aluminum agglomeration of AP/HTPB composite propellant. *Acta Astronaut.* **2019**, *156*, 14–22. [CrossRef]
12. Tu, C.Y.; Chen, X.; Li, Y.K.; Zhang, B.C.; Zhou, C.S. Experimental study of Al agglomeration on solid propellant burning surface and condensed combustion products. *Def. Technol.* **2022**, *5*, 2214–9147. [CrossRef]
13. Tu, C.; Zhuang, Y.; Li, Y.; Zhou, C.; Cai, W.; Chen, X.; Li, W. Combustion Process and Aluminum Agglomeration Characteristics of NEPE Propellant. *J. Aerosp. Power* **2022**, *10*, 1–8.
14. Tu, C.; Lin, Z.; Dong, L.; Zhuang, Y.; Li, Y.; Zhou, C.; Cai, W.; Chen, X. Dynamic Behavior Study of Aluminum Aggregates on NEPE Propellant Combustion Surface. *J. Propuls. Technol.* **2022**, *11*, 1–10.
15. Liu, Z.; Li, S.; Liu, M.; Guan, D.; Sui, X.; Wang, N. Experimental investigation of the combustion products in an aluminised solid propellant. *Acta Astronaut.* **2017**, *133*, 136–144. [CrossRef]
16. Zhou, X.; Zou, M.; Huang, F.; Yang, R.; Guo, X. Effect of organic fluoride on combustion agglomerates of aluminized HTPB solid propellant. *Propellants Explos. Pyrotech.* **2017**, *42*, 417–422. [CrossRef]
17. Gallier, S. A stochastic pocket model for aluminum agglomeration in solid propellants. *Propellants Explos. Pyrotech.* **2009**, *34*, 97–105. [CrossRef]
18. Gnanaprakash, K.; Chakravarthy, S.R. Effect of binder melt flow on the leading edge flames of solid propellant sandwiches. *Proc. Combust. Inst.* **2019**, *37*, 3127–3134. [CrossRef]
19. Chen, Y.; Zhu, B.; Sun, Y.; Zhang, S.; Shi, W.; Liu, X. Effects of ammonium perchlorate particle size on the aluminum agglomeration in primary combustion of the ammonium perchlorate/ aluminum binary mixture with a high aluminum content. *Energy Fuels* **2019**, *33*, 9302–9308. [CrossRef]
20. Li, L. *Experimental and Numerical Study of Combustion and Particle Agglomeration Characteristics of Solid-Fueled Ram Engines*; Nanjing Unversity of Science and Technology: Naniing, China, 2019.
21. Grigor'Ev, V.G.; Kutsenogii, K.P.; Zarko, V.E. Model of aluminum agglomeration during the combustion of a composite propellant. *Combust. Explos. Shock Waves* **1981**, *17*, 356–363. [CrossRef]
22. Li, L.B.; Chen, X.; Zhou, C.S.; Li, W.X.; Zhu, M. Experimental and model investigation on agglomeration of aluminized fuel-rich propellant in solid fuel ramjet. *Combust. Flame* **2020**, *219*, 437–448. [CrossRef]
23. Duterque, J.; Propulsion, C. Experimental studies of aluminum agglomeration in solid rocket motors. *Int. J. Energetic Mater. Chem. Propuls.* **1997**, *4*, 693–705. [CrossRef]